ARMY RESEARCH LABORATORY

Nondestructive Characterization of Low-Velocity Impact Damage in Protective Ceramic Components

by Raymond E. Brennan, William H. Green, and Constantine G. Fountzoulas

ARL-TR-6700 **September 2013**

NOTICES

Disclaimers

The findings in this report are not to be construed as an official Department of the Army position unless so designated by other authorized documents.

Citation of manufacturer's or trade names does not constitute an official endorsement or approval of the use thereof.

Destroy this report when it is no longer needed. Do not return it to the originator.

Army Research Laboratory
Aberdeen Proving Ground, MD 21005-5069

ARL-TR-6700 **September 2013**

Nondestructive Characterization of Low-Velocity Impact Damage in Protective Ceramic Components

Raymond E. Brennan, William H. Green, and Constantine G. Fountzoulas
Weapons and Materials Research Directorate, ARL

REPORT DOCUMENTATION PAGE	Form Approved OMB No. 0704-0188

1. REPORT DATE *(DD-MM-YYYY)*	2. REPORT TYPE	3. DATES COVERED (From - To)
September 2013	Final	September 2011–September 2012

4. TITLE AND SUBTITLE
Nondestructive Characterization of Low-Velocity Impact Damage in Protective Ceramic Components

5a. CONTRACT NUMBER

5b. GRANT NUMBER

5c. PROGRAM ELEMENT NUMBER

6. AUTHOR(S)
Raymond E. Brennan, William H. Green, and Constantine G. Fountzoulas

5d. PROJECT NUMBER
MMCE14-2010

5e. TASK NUMBER

5f. WORK UNIT NUMBER

7. PERFORMING ORGANIZATION NAME(S) AND ADDRESS(ES)
U.S. Army Research Laboratory
ATTN: RDRL-WMM-D
Aberdeen Proving Ground, MD 21005-5069

8. PERFORMING ORGANIZATION REPORT NUMBER
ARL-TR-6700

9. SPONSORING/MONITORING AGENCY NAME(S) AND ADDRESS(ES)

10. SPONSOR/MONITOR'S ACRONYM(S)

11. SPONSOR/MONITOR'S REPORT NUMBER(S)

12. DISTRIBUTION/AVAILABILITY STATEMENT
Approved for public release; distribution is unlimited.

13. SUPPLEMENTARY NOTES

14. ABSTRACT
In theater, protective systems are exposed to a wide variety of ballistic and sub-ballistic threats, which may compromise their ability to withstand single or multiple impacts. Low-velocity impact damage can originate from a number of sources that may include vehicle collisions, harsh terrain and environmental conditions, or foreign object debris from persons of interest, other vehicles, or shrapnel. Advanced ceramic components in these systems include materials, such as aluminum oxide, boron carbide, and silicon carbide. By subjecting these components to experimentally controlled low-velocity impacts and using nondestructive bulk characterization techniques to detect resulting surface and internal damage, a comparison of baseline and damaged states can be established. By developing models to simulate impact events and replicate fracture patterns, the experimental time and cost can be reduced. These methods can be used to establish a relationship between processing or manufacturing defects in these materials and determine the mechanisms that cause damage (i.e., crack initiation and crack propagation) to provide insight into development of improved materials. By qualitatively and quantitatively characterizing these components before and after impact, materials can be ranked and down selected according to their ability tolerate damage, and leading candidates can be implemented for direct improvement of protective systems.

15. SUBJECT TERMS
impact, damage, ultrasound, quantitative, modeling

16. SECURITY CLASSIFICATION OF:			17. LIMITATION OF ABSTRACT	18. NUMBER OF PAGES	19a. NAME OF RESPONSIBLE PERSON
a. REPORT	b. ABSTRACT	c. THIS PAGE			Raymond E. Brennan
Unclassified	Unclassified	Unclassified	UU	22	19b. TELEPHONE NUMBER (*Include area code*) 410-306-0913

Standard Form 298 (Rev. 8/98)
Prescribed by ANSI Std. Z39.18

Contents

List of Figures

List of Tables

Acknowledgments

The authors would like to acknowledge James Wolbert and Jian Yu of the U.S. Army Research Laboratory (ARL) for their efforts and support.

1. Introduction

Weight reduction is desirable for vehicle systems to increase maneuverability and transportability while reducing operational costs. The implementation of ceramic and composite materials into opaque protective systems traditionally dominated by metals has been initiated to reduce the weight of these systems. These opaque systems typically consist of multiple layers of metal, ceramic, or composite materials that are stacked and adhered by polymer interlayers. In these complex systems, the presence of internal defects, such as pores, inclusions, or secondary phases in the individual layers cannot be detected by simple visual inspection. For these multilayer systems, internal defects, such as delaminations and disbonds at various interfaces can lead to a reduction in stiffness and weaken the overall system *(1−6)*, but they cannot be detected visually. Advanced nondestructive bulk characterization of these types of processing or manufacturing inhomogeneities is necessary for the establishment of baseline conditions for opaque materials.

Although nondestructive bulk characterization techniques can be utilized in the pre-impacted state to detect material inhomogeneities and improve quality control for opaque protective systems before they are utilized in the field, they can also be used post-impact to detect resulting damage or to compare baseline and damaged states for the determination of critical impact conditions. This study will focus on a comparison of ceramic components used in opaque protective systems and their ability to withstand low-velocity impact damage. Success will be measured quantitatively by volume percent damage as determined through nondestructive means. In addition, to lower the experimental costs for current and future target architectures, modeling will be used to simulate the damage from cracking and delamination of the targets.

2. Experimental

The targets chosen for this study were 15.24 × 15.24 × 3.18 cm. Each target contained a 10.16 × 10.16 × 1.27 cm ceramic tile surrounded by four 2.54 × 12.7 × 1.27 cm 1018 cold finished mild steel bars. The ceramic and steel surrounds were backed by a 15.24 × 15.24 × 1.91 cm 5083-H131 aluminum plate. The layers were bonded together using 0.06 cm thermoplastic polyurethane adhesive film layers. Although the steel and aluminum backing materials were the same for each target, four different types of ceramic materials were used to compare their performance against low-velocity impact threats. Aluminum oxide (alumina), solid-state sintered silicon carbide (sintered SiC), hot-pressed SiC, and boron carbide (B_4C) were the ceramics of

choice. Up to seven targets of each type were fabricated for testing under different velocity and energy conditions.

3. Destructive and Nondestructive Testing Methods

Fragment simulating projectile (FSP) testing was chosen as the destructive testing method for producing low-velocity impact damage in the targets. This method utilized a pneumatic launcher to fire 17 0.22 cal (1.1 g) fragment simulating projectiles into the center of each target. The average impact velocities for the five sets of FSP tests were ~140, 230, 300, 450, and 550 m/s.

Ultrasound characterization was used to nondestructively detect material variations, defects, and damage in the ceramic tiles. As the acoustic waves were transmitted into the panels, material changes in individual ceramic or metal layers (pores, inclusions, cracks) or interlayers (disbonds, delaminations) resulted in acoustic impedance mismatches that caused reflection of the waves (*7–9*). Spatial maps, or ultrasound C-scan images, of the gated signals were used to form visual plots of acoustic variations caused by defects and/or damage. Ultrasonic testing was conducted using an Olympus 10 MHz longitudinal immersion transducer mounted to a Mistras Group conventional ultrasound scanning system.

A previously developed technique was implemented for quantitatively estimating the percent damage in targets subjected to low-velocity impact testing (*10*). This method was applied to C-scan images in which the bottom surface signal amplitude was mapped to represent volumetric damage through the bulk of each target.

4. Qualitative and Quantitative Damage Analysis

FSP testing was conducted on five targets of each material at average impact velocities ranging from ~140 to 550 m/s and average impact energies ranging from ~6 to 107 J. Two different types of ultrasound C-scan images were collected through the strike face of each target. The first type of image was collected by gating, or selecting, the top surface signal reflection from the target and monitoring changes in signal amplitude to characterize surface and near-surface features. Figure 1 shows the post-impact surface/near-surface C-scan images of 20 targets, representing the four different ceramic materials at five different FSP velocities. For the first two average velocities of 140 and 230 m/s, there was no visible surface or near-surface damage to any of the targets. At 300 m/s, damage to the impact site was evident in the sintered SiC and B_4C targets, but this was limited to small surface indentations. Although the alumina target showed no

qualitative damage at the point of impact, inhomogeneities, such as inclusions and pores, were present throughout the ceramic. When the FSP velocity was increased to 450 m/s, damage to the impact site was evident in all four materials, with the damage slightly larger for the sintered SiC and B_4C targets. The sintered SiC target also showed additional spalling damage, which was confirmed by material loss to the surface after visual observation. At the highest velocity of 550 m/s, the damage did not appear to increase significantly for the alumina and hot-pressed SiC targets. However, the sintered SiC target showed a high degree of surface damage from spalling, and the B_4C target started to show evidence of hairline surface cracking. Although these surface/near-surface results were consistent with qualitative visual observation of the targets, the more interesting results came from the second type of the C-scan images, which revealed hidden bulk damage.

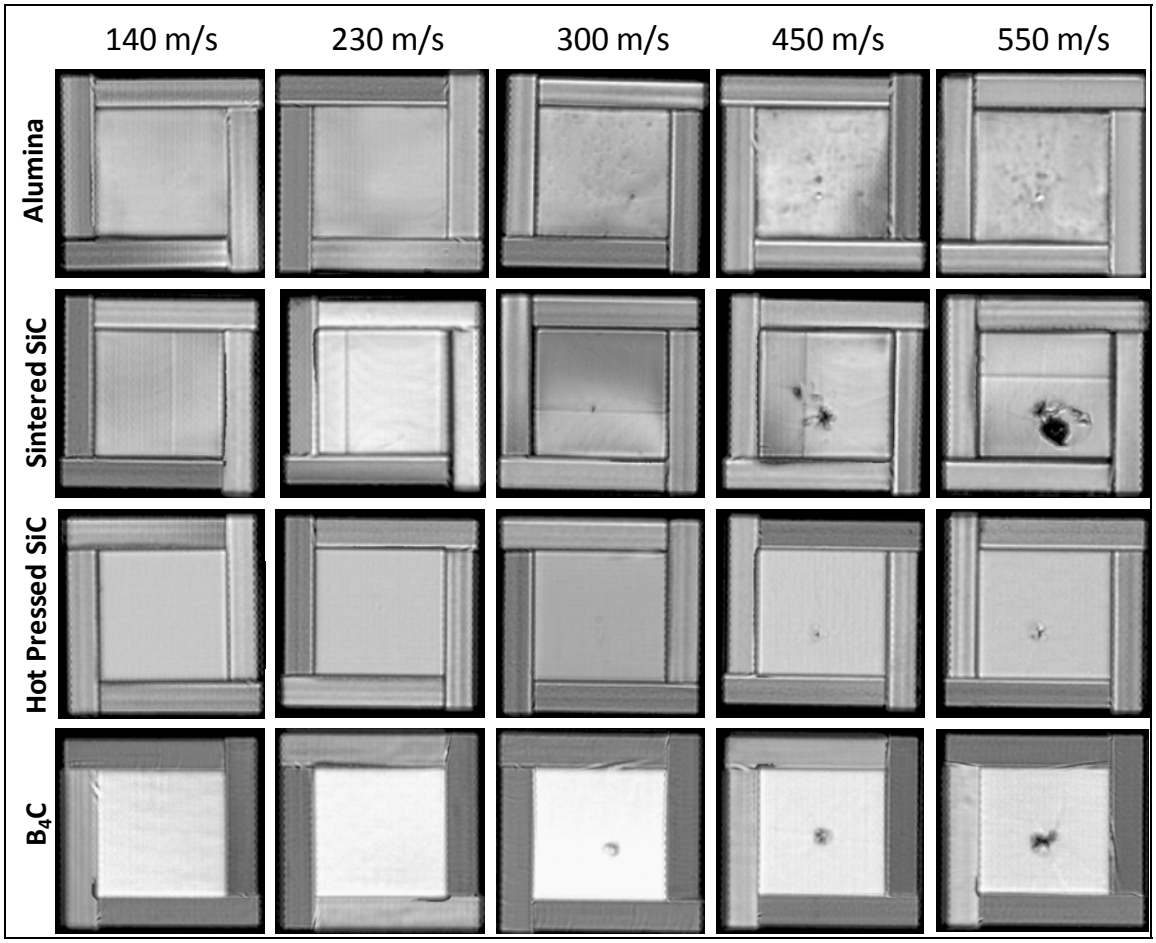

Figure 1. Surface/near-surface C-scan images of 20-target matrix.

The second type of C-scan image was collected by gating the bottom surface signal reflection of the ceramic component and monitoring changes in signal amplitude to characterize the volumetric damage. Figure 2 shows the post-impact bulk C-scan images of the 20-target matrix. Unlike the minor damage observed in the surface/near-surface scans, the bulk damage to all the

ceramic components was significantly larger, even at the lowest velocities. At 140 m/s, the lowest FSP velocity, the damage trends were similar to the surface/near-surface targets, with the sintered SiC and B_4C targets showing a higher degree of impact damage. The sintered SiC sample exhibited partial radial cracking originating from what appeared to be a cone crack at the point of impact. Similar patterns of circular damage at the point of impact from other studies have been analyzed using x-ray computed tomography through the cross section, and cone cracks were often located in these regions (*11*). At 230 m/s, partial radial cracking was evident in the bulk of all four ceramic materials. Qualitatively, the degree of volumetric damage appeared to be less for the alumina and hot-pressed SiC targets. When increasing the FSP velocity to 300 and 450 m/s, the impact damage region became larger and larger, with the radial cracks propagating to the edge of the ceramic tiles. The number of radial cracks, radial crack widths, and cone crack diameters appeared to increase at higher velocities. At the highest FSP velocity of 550 m/s, the most severe damage was evident in the sintered SiC sample, which also showed a high degree of surface spalling in the corresponding surface/near-surface C-scan image. Although the trends remained the same throughout both sets of C-scan images, the hidden internal damage was not effectively demonstrated until the bulk scans revealed the true damage state in each target.

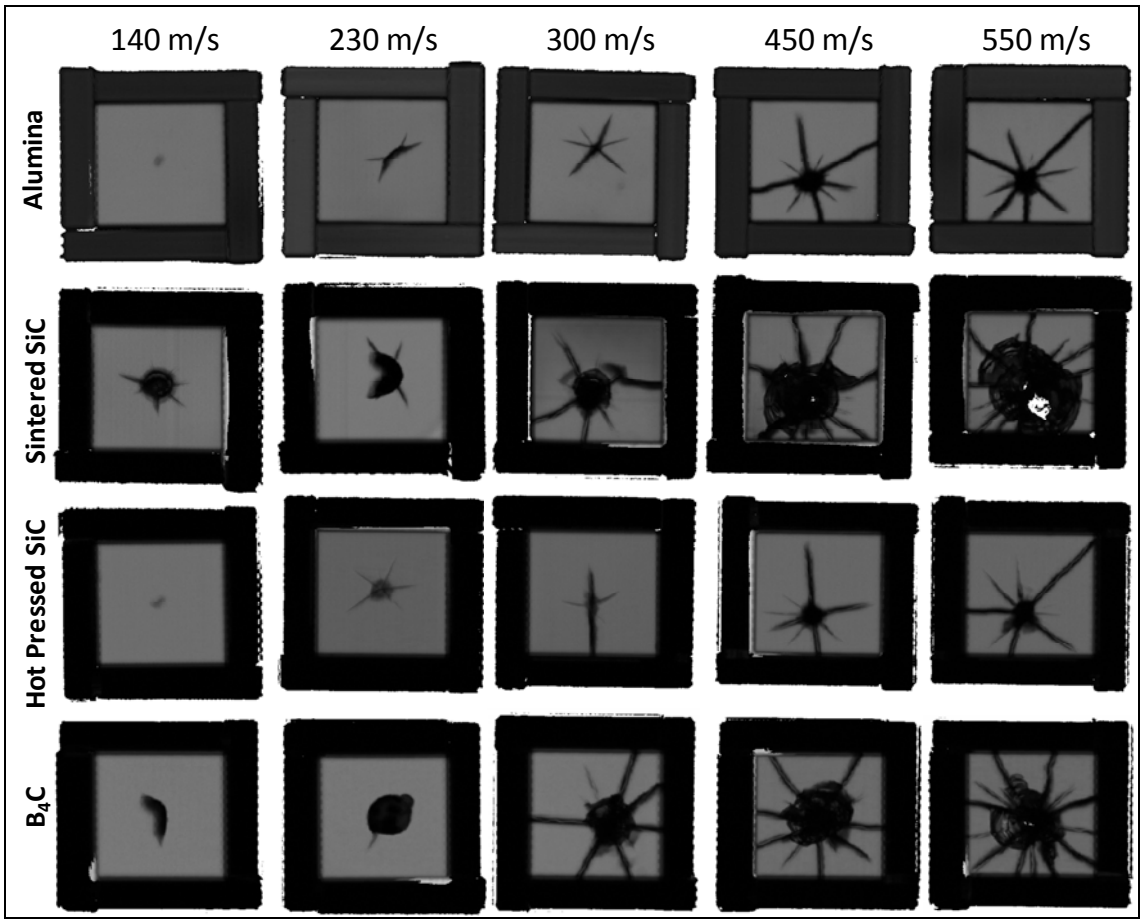

Figure 2. Bulk C-scan images of 20-target matrix.

Quantitative data was collected from the C-scan images for each target. First, the velocity and energy conditions for each FSP test were recorded. Next, the damage type was identified, including indents at the point of impact, partial radial cracks, and full radial cracks that propagated to the edge of the ceramic. Although it was suspected that they were present in many of the targets, cone cracks were not categorized because cross-sectional imaging was not performed on all targets to confirm whether or not the circular damage at the point of impact was a cone crack or a large indent. The number of partial and full radial cracks was identified. Finally, the aforementioned quantitative histogram was applied to the bulk C-scan image data in order to estimate the volumetric percent damage (*10*). Each bulk C-scan damage map was processed using an inverted grayscale, and histograms of the maps were plotted as a function of the grayscale levels. A threshold was chosen on the histogram in which any occurrences to the right side represented the damaged regions of the target and any occurrences to the left side represented the undamaged regions. The summation of total number of occurrences representing the damaged regions was calculated, and this value was divided by the total number of occurrences in the image and multiplied by 100 to acquire the estimated percent damage in the selected panel.

The percent damage data and other quantitative data were evaluated with respect to the velocity, energy, and damage conditions at which different damage types occurred. An example of one of these quantitative assessments is shown in table 1, which shows the B_4C target data. Figure 3 shows the corresponding histograms that were used to determine the percent damage values. The left tail of the histogram plot, which represented the occurrences of damage, continued to grow as the velocities and energies were increased. The threshold for significant damage was identified at the transition between partial radial cracking and full radial cracking. This occurred between velocities of 229 and 315 m/s and energies from 18.1 to 34.2 J for targets containing B_4C ceramic components. Table 2 shows the quantitative results for all four target types at the highest FSP velocity of ~550 m/s. When comparing the four different types of ceramics, the percent damage values were much higher for B_4C at 42.32% and sintered SiC at 61.20% than they were for alumina at 16.05% and hot-pressed SiC at 15.65%. The higher damage percentages also corresponded to more full radial cracks that propagated to the edge of the ceramics, as sintered SiC and B_4C had 8 and 12 cracks, respectively, whereas hot-pressed SiC and alumina had 3 and 4 cracks, respectively.

Table 1. Quantitative data collected for B_4C targets.

Sample	Velocity (m/s)	Energy (J)	Percent Damage	No. Partial Cracks	No. Full Cracks	Class
B_4C-12	137	6.475	5.23	0	0	Indent
B_4C-10	229	18.092	11.98	1	0	Radial partial
B_4C-3	315	34.233	23.39	3	6	Radial edge
B_4C-2	447	72.053	36.19	3	8	Radial edge
B_4C-1	547	107.036	42.32	1	12	Radial edge

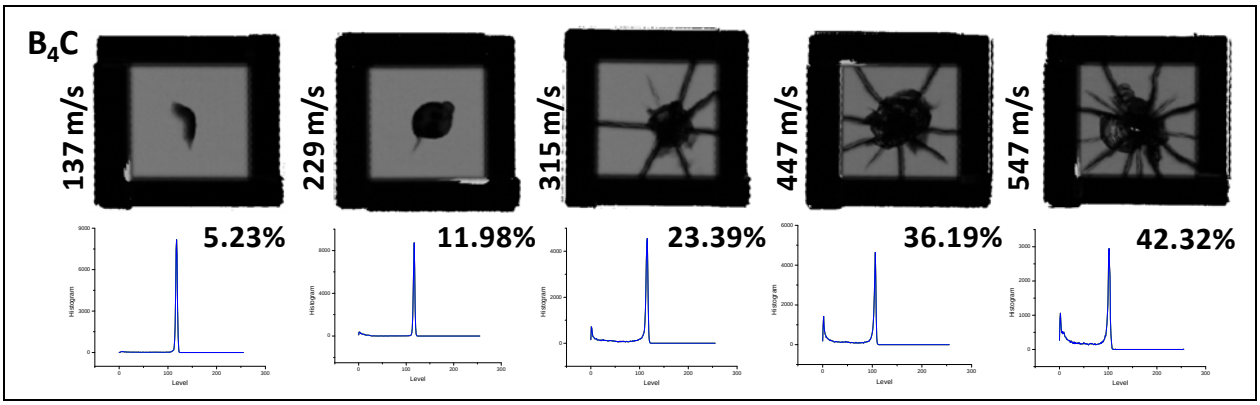

Figure 3. Histogram method applied to B_4C targets.

Table 2. Quantitative data collected for targets at v~550 m/s.

Sample	Velocity (m/s)	Energy (J)	Percent Damage	No. Partial Cracks	No. Full Cracks	Class
B_4C-12	137	6.475	5.23	0	0	Indent
B_4C-10	229	18.092	11.98	1	0	Radial partial
B_4C-3	315	34.233	23.39	3	6	Radial edge
B_4C-2	447	72.053	36.19	3	8	Radial edge

Although the tables showed a point-by-point comparison of quantitative damage for the ceramic components from various targets, plots of damage percent against impact energy in figure 4 revealed the evolution of trends over the full dynamic range of FSP testing. At lower impact energies, damage to the alumina and hot-pressed SiC targets was minimal, and even as the energy was increased to above 100 J, the damage percent did not eclipse 20% for either material. In contrast, the B_4C and sintered SiC targets were much more susceptible to damage under comparable conditions, exhibiting damage percentages above 20% at impact energies as low as 30 J. As the impact energies increased to ~70 J, B_4C and sintered SiC damage further increased to 36.19% and 46.18%, respectively, as hot-pressed SiC and alumina remained at 13.57% and 13.93%, respectively. As mentioned previously, under the highest velocity and energy conditions tested, the sintered SiC targets sustained the highest degree of damage compared to the other materials. Although sintered SiC showed the poorest performance against higher energy threats, several tests at impact energies below 20 J revealed less damage for sintered SiC when compared to the other materials. As evidenced by the plot, two of the sintered SiC targets tested below 20 J had damage percentages below 3% whereas two targets had damage percentages above 9%, including the target impacted at the lowest energy of 6.5 J, which had a damage percent of 9.48%. This level of inconsistency was unique to the sintered SiC material, as all of the other materials exhibited increasing damage percentages with increasing impact energies. One explanation may have been attributed to a greater flaw dependency for the sintered SiC, which contained no glassy phase, in opposition to the hot-pressed SiC. This could have led to increased variability and inconsistent performance from target-to-target. However, the lower damage

results could have also been anomalies that might have required repeat tests under like conditions to enhance their statistical significance. In any case, the overall trends in the plots allowed the four materials to be ranked against each other in terms of damage response against low-velocity impact threats, with alumina and hot-pressed SiC showing a much higher damage tolerance than B_4C and sintered SiC.

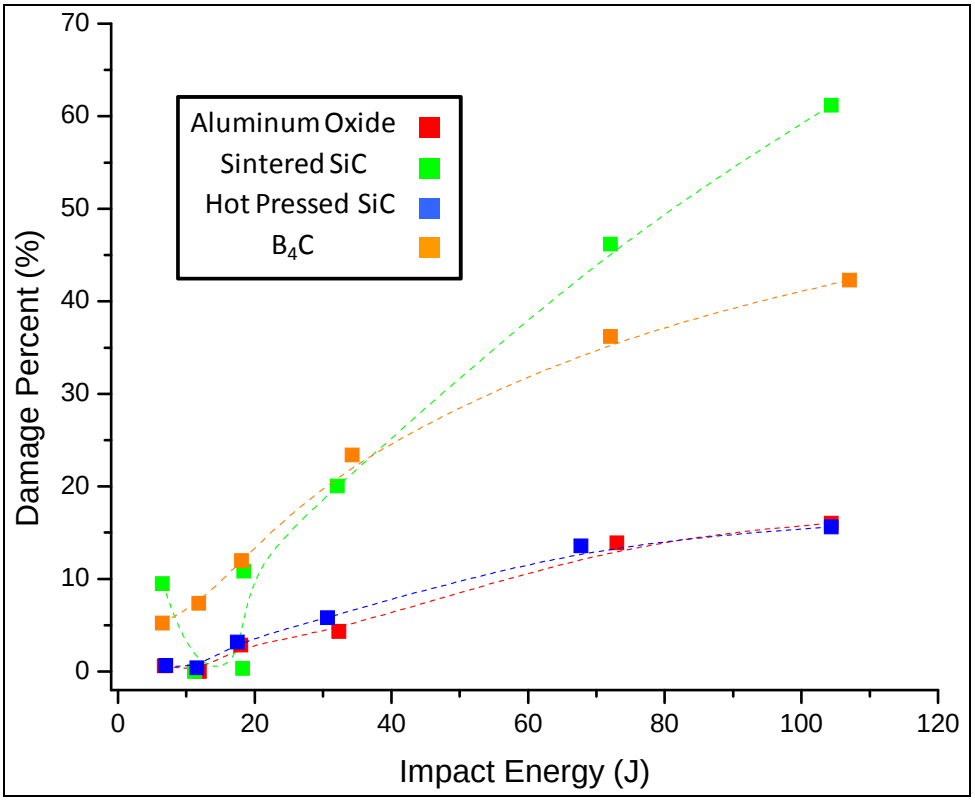

Figure 4. Comparison of material damage response under FSP testing.

5. Modeling and Simulation of Target Failure

Modeling has been shown repeatedly as a means of cutting experimental cost for the improvement of current target architectures and as a preselecting tool of future architectures. The dynamic behavior of alumina and sintered SiC targets (figure 5) was studied by three-dimensional models and simulated using the nonlinear commercial package ANSYS/AUTODYN (*11*). The geometry of the modeled targets was identical to the actual geometry (figure 5).

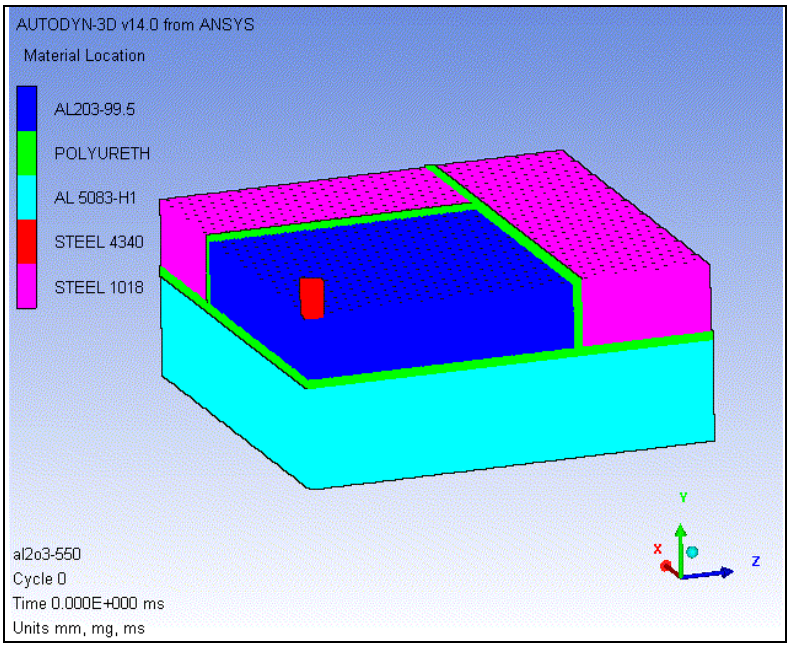

Figure 5. Target modeled architecture testing.

Table 3 shows the material models used, which were obtained from the AUTODYN library (*11*). Using the geometry detailed above, all materials were modeled using the Smooth Particle Hydrodynamic (SPH) solver. The SPH particle size was 0.75 for the aluminum and steel, 0.5 for the ceramics, and 0.25 mm for the FSP and polyurethane. The symmetry of the modeling was set to axi-symmetric.

Table 3. Summary of Equation of State (EOS), strength and failure material models used (Johnson−Holmquist [JH]2 and Johnson−Cook [JC]).

	Al_2O_3	**Sintered SiC**	**Aluminum**	**Steel (Frame)**	**Steel (FSP)**	**PU**
EOS	Polynomial	Polynomial	Shock	Linear	Shock	Linear
Strength	JH2	JH2	Steinberg Guinam	JC	JC	Elastic
Failure	JH2	JH2	None	None	None	Stress

Figures 6 and 7 show the simulated damage across the ceramic surface and along its cross section, respectively, for the alumina targets at impact speeds of 300, 450, and 550 m/s. Although the simulations duplicated the longer radial cracks well, the smaller cracks were not predicted. The simulations showed increasing damage at the point of impact and increased crack propagation at increasing impact velocities, which was in agreement with the experimental results. However, whereas the simulations show symmetrical cracks, due to the axi-symmetry of the modeling, the experimental results were different due to eccentric impact of the targets. At an impact velocity of 300 m/s, the simulations predicted the curvature of the long cracks, and the propagation of the cracks, which were also demonstrated by the nondestructive evaluation (NDE) results. As the impact velocity increased, the experimental and simulated cracks become

linear until they reached the edge of the ceramic target. The authors believe that further modification of the existing strength and failure material models of alumina will allow accurate prediction of the smaller cracks detected by the NDE techniques. Modeling and simulation enabled the testing of a much wider set of parameters and conditions without using the extensive time and resources that were required to run the same types of tests experimentally. This was demonstrated by simulating an FSP impact at a velocity of 800 m/s (figures 6–7), which was a condition that could not be achieved by the current experimental FSP capabilities. Under the higher impact velocity, the simulation showed increased damage and additional stresses that started to develop around both the impact center and near the edge of the ceramic.

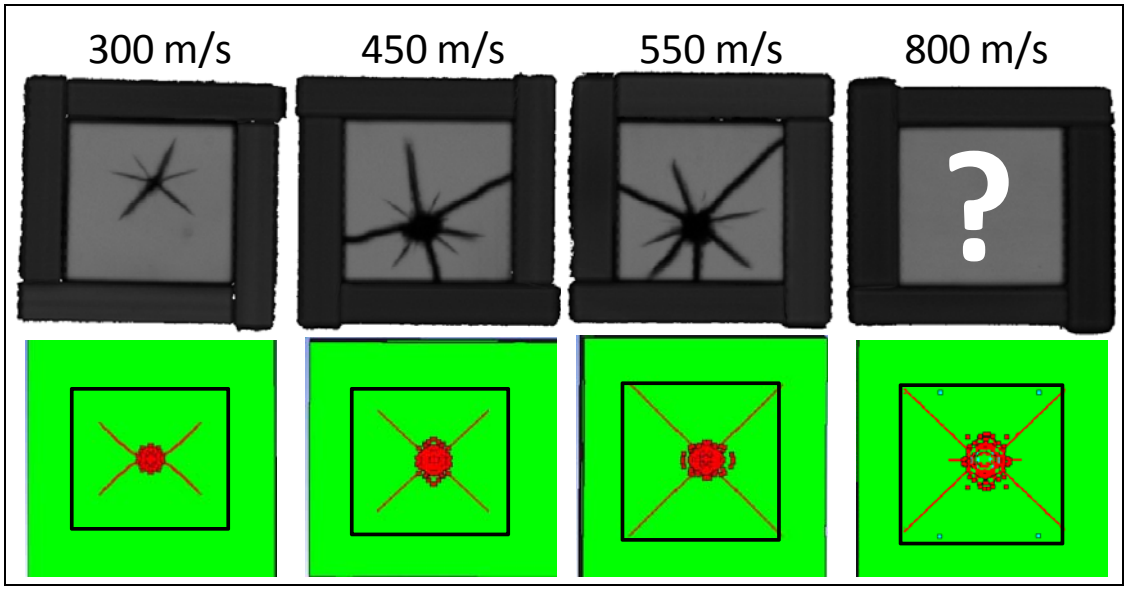

Figure 6. Experimental (top) and simulated (bottom) impact damage at 70 µs to alumina targets. Velocity of 800 m/s could be simulated but not experimentally tested.

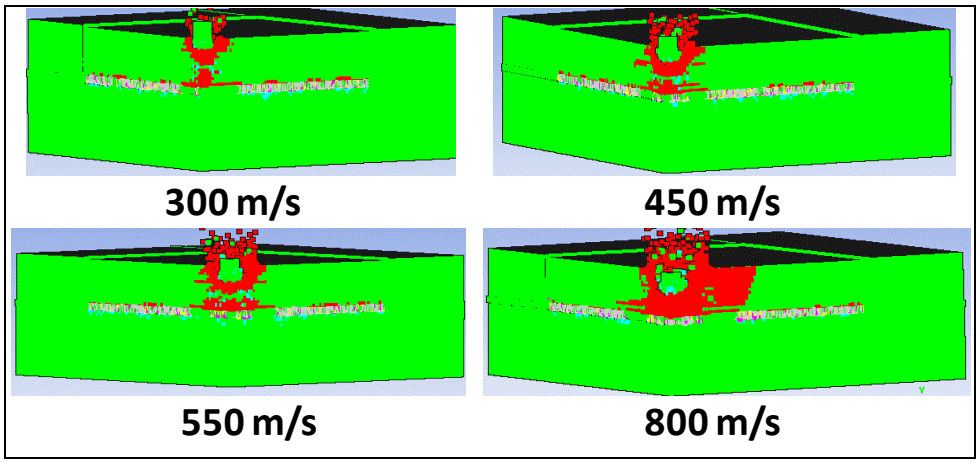

Figure 7. Cross sections of simulated impact damage to alumina targets (70 µs).

In addition to the alumina targets, simulations were also run for sintered SiC samples at 450 and 550 m/s to compare materials that exhibited drastically different damage behavior experimentally. The bulk C-scan images and simulated top view and cross-sectional images are shown at the two velocities in figure 8. At 450 m/s, the simulations showed the development of both radial and cone cracks, which was consistent with the corresponding C-scan image. At 550 m/s, the number and severity of radial and cone cracks increased, with the cross-sectional simulation showing severe damage at both the point of impact and the edge of the sintered SiC target. In contrast to simulations of the alumina targets, the sintered SiC simulations showed evidence of cone cracking and increased amounts of damage under the same velocity conditions. The successful prediction of the damage to the sintered SiC may be attributed to the previously successful modification of SiC material strength and failure models available in open literature. The authors believe that an experimental impact at the geometric center of the ceramic would have produced damage similar to the simulated failure results. This information was valuable for assessing damage evolution trends for the different materials. Both sets of simulations compared well with their experimental counterparts. Because the simulated sintered SiC targets showed a fracture pattern and degree of damage variations compared to the simulated alumina targets, and other conditions including target dimensions, backing and supporting materials, and FSP testing conditions remained the same, performance differences were directly related to the type of ceramic material used. A combination of experimental and modeling results can be crucial in determining the failure mechanisms of the materials studied, which is expected to produce better designs at a lower cost.

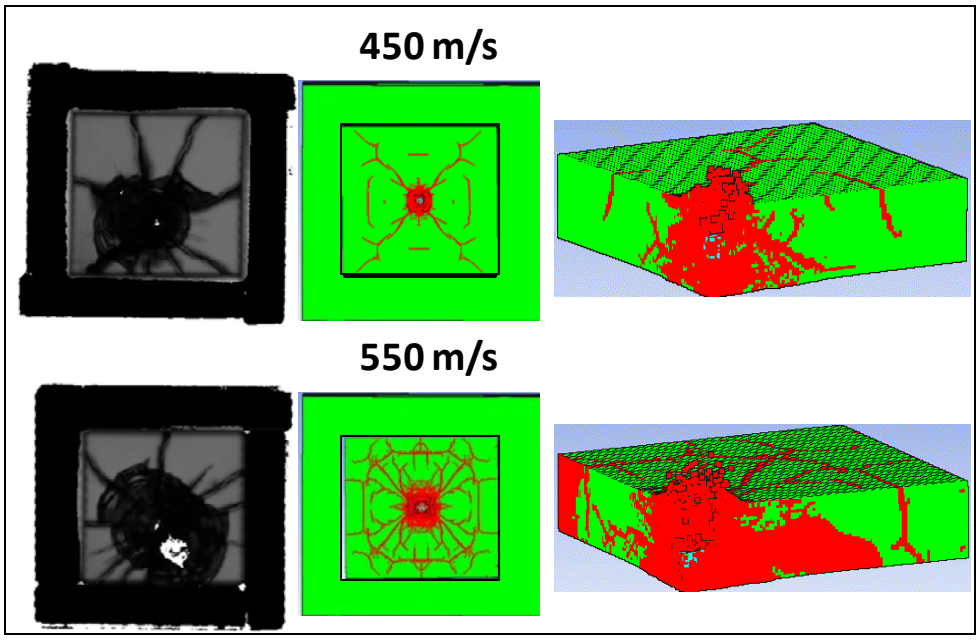

Figure 8. Experimental and simulated (70 μs) impact damage comparisons for sintered SiC targets.

6. Summary and Conclusions

Targets containing four different types of ceramic components, including alumina, sintered SiC, hot-pressed SiC, and B_4C, were tested under low-velocity FSP conditions to determine the effect of impact energy on damage. Experimental studies were performed by increasing the velocity and energy conditions through FSP testing. Ultrasound C-scan imaging was used to generate qualitative damage maps and a quantitative ultrasound histogram technique was utilized to estimate volume percent damage through the bulk of each target. Damage was classified as either small indent damage at the point of impact, partial radial cracking, or full radial cracking out to the edge of the ceramic. A bulk failure model was developed to simulate the conditions used for experimental testing and to explore conditions that could not be accomplished through experimental means. Both experimental and modeling results showed agreement in ranking the performance of ceramic materials, with hot-pressed SiC and alumina demonstrating the highest damage tolerance, followed by B_4C, and finally sintered SiC, which was most susceptible to radial cracking damage after low-velocity impact. The qualitative damage patterns from the C-scan images and simulations also compared favorably under like conditions in terms of severity and type of damage sustained. Quantitatively, under the highest experimental velocity conditions of 550 m/s, which corresponded to impact energy values on the order of ~105 J, the damage percentages were 15.65% for hot-pressed SiC, 16.05% for alumina, 42.32% for B4C, and 61.20% for sintered SiC. Controlled destructive testing, nondestructive evaluation, and modeling and simulation methods successfully provided qualitative comparisons and quantifiable metrics to successfully rank ceramic components in terms of predicted performance against low-velocity impact damage. Application of these improved configurations for the down selection of a protective system component used in vehicles should help to improve damage tolerance and enhance protective capabilities for Soldiers in the field.

The simulations of the damage of sintered SiC at various impact speeds were more successful than the alumina simulations. This was attributed to the production of modified material models for SiC (*12−13*). Efforts to produce better material models of alumina and especially for the challenging boron carbide are currently ongoing.

7. References

1. Anderson, C. E.; Walker, J. D.; Lankford, J. *Investigations of the Ballistic Response of Brittle Materials*; SwRI Project 06-5117/002; U.S. Army Research Office, 1995, 1–112.
2. Bourne, N.; Millett, J.; Rosenberg, Z.; Murray, N. 1998. "On the Shock Induced Failure of Brittle Solids. *Journal of the Mechanics and Physics of Solids* **1998**, *46* (10), 1887–1908.
3. Sherman, D. Impact Failure Mechanisms in Alumina Tiles on Finite Thickness Support and the Effect of Confinement. *International Journal of Impact Engineering* **2000**, *24* (3), 313–328.
4. Sherman, D.; Ben-Shushan, T. Quasi-Static Impact Damage in Confined Ceramic Tiles. *International Journal of Impact Engineering* **1998**, *21* (4), 245–265.
5. McMichael, S.; Fischer, S. Understanding Materials with Instrumented Impact. *ME* **1989**, 47–50.
6. Chacon-Nava, J. G.; Stott, F. H.; de la Torre, S. D.; Martinez-Villafane, A. Erosion of Alumina and Silicon Carbide at Low-Impact Velocities. *Materials Letters* **2002**, *55*, 269–273.
7. Mix, P. E. *Introduction to Nondestructive Testing*, John Wiley & Sons, 1987, 104–153.
8. Krautkramer, J.; Krautkramer, H. *Ultrasonic Testing of Materials*, Springer−Verlag, 1990; 1−50.
9. Bhardwaj, M. C. *Ceramic Monographs – Handbook of Ceramics*, 41(1), 1992.
10. Brennan, R. E. *Quantitative Histogram Damage Assessment Method for Low Velocity Impact of Transparent Materials*; ARL-TN-0438; U.S. Army Research Laboratory: Aberdeen Proving Ground, MD, 2011; 1–5.
11. ANSYS/AUTODYN Vol. 12.1. Manual, Century Dynamics Inc., Concord, CA.
12. Fountzoulas, C. G.; Cheeseman, B. A.; LaSalvia J. C. *Simulation of Ballistic Impact of a Tungsten Carbide Sphere on a Confined Silicon Carbide Target*; ARL-RP-250; U.S. Army Research Laboratory: Aberdeen Proving Ground, MD.
13. Fountzoulas C. G.; LaSalvia. *Improved Modeling and Simulation of the Ballistic Impact of Tungsten-Based Penetrators on Confined Hot-Pressed Boron Carbide Targets*, Advances in Ceramics VIII, Wiley Online Library, 209–217).

List of Symbols, Abbreviations, and Acronyms

ARL	U.S. Army Research Laboratory
B_4C	boron carbide
EOS	Equation of State
FSP	fragment simulating projectile
NDE	nondestructive evaluation
SiC	silicon carbide
SPH	Smooth Particle Hydrodynamic

NO. OF COPIES	ORGANIZATION
1 (PDF)	DEFENSE TECHNICAL INFORMATION CTR DTIC OCA
1 (PDF)	DIRECTOR US ARMY RESEARCH LAB IMAL HRA
1 (PDF)	DIRECTOR US ARMY RESEARCH LAB RDRL CIO LL
1 (PDF)	GOVT PRINTG OFC A MALHOTRA

ABERDEEN PROVING GROUND

3 (PDF)	RDRL WMM D R BRENNAN W GREEN RDRL WMM B C FOUNTZOULAS